High Speed Imaging of Bubble Clouds in Pulsed Cavitational Ultrasound Therapy - Histotripsy

Zhen Xu[1], Mekhala Raghavan[1], Timothy L. Hall[1], Ching-Wei Chang[1],
Mary-Ann Mycek[1], J. Brian Fowlkes[2], Charles A. Cain[1]
[1]Department of Biomedical Engineering, University of Michigan, Ann Arbor, MI 48109
[2]Department of Radiology, University of Michigan, Ann Arbor, MI 48109

***Abstract*—Our investigations have shown that short (≤50 μsec) high intensity, low duty cycle ultrasound pulses can achieve significant breakdown of tissue structure at a tissue-fluid interface and in bulk soft tissue. We call this technique "histotripsy", and inertial cavitation is its hypothesized mechanism. To understand the physical basis of histotripsy, a high speed camera was used to image hypothesized bubble clouds generated by ultrasound pulses. The results show the following: (1) Ultrasound pulses generated a bubble cloud both at a tissue-water interface and inside a gel used to mimic the bulk soft tissue. This bubble cloud plays an important role in the histotripsy process; (2) An ultrasound pulse of several μsec long can generate a bubble cloud lasting for several hundreds of μsec; and (3) the intensity threshold to initiate a bubble cloud is lower at a gel-water interface than inside a gel.**

Keywords-cavitation; bubble imaging; pulsed ultrasound; tissue erosion; tissue homogenization; histotripsy

I. INTRODUCTION

Our recent investigations have shown that pulsed ultrasound at high acoustic intensities can achieve significant breakdown of tissue structure. We call this technique "histotripsy". At a tissue-water interface, histotripsy produces effective tissue removal resulting in clearly demarcated perforations [1]. In bulk tissue, histotripsy produces "complete" fractionation of tissue volumes, resulting in a cavity containing a smooth uniform liquid [2, 3].

The primary mechanism for histotripsy is believed to be inertial cavitation. This is supported by an high amplitude, temporally changing acoustic backscatter of therapy ultrasound pulses observed during the histotripsy process [4, 5], which is an acoustic signature of cavitation. No visually observable tissue disruption is produced without initiation of a temporally-spatially variable in backscatter pattern.

We hypothesize that this backscatter pattern is the result of sound reflection from a dynamically changing cluster of bubbles (bubble cloud) generated by high intensity ultrasound pulses. In this paper, we employed high-speed imaging to observe the hypothesized bubble clouds generated by short, high intensity ultrasound pulses, and correlated with simultaneously collected acoustic backscatter signals. In addition, we imaged the bubble cloud changes during and after the ultrasound pulses. The results help us further understand the histotripsy mechanism.

II. METHODS

A. Ultrasound Generation

Ultrasound pulses were generated by an 18-element spherical-shell therapeutic array (Imasonic, S.A., Besançon, France) with a center frequency of 750-kHz and a focal length of 100-mm. The therapy array has an annular configuration with outer and inner diameters of 145 and 68 mm. A PC console provided control of the array and a motorized 3-D positioning system (Parker Hannifin, Rohnert Park, CA USA) to position it. The pressure waveform at the focus of the array in the acoustic field was measured in degassed water using a fiber-optic probe hydrophone (FOPH) [6] developed in-house. The acoustic parameters used are listed in Table 1.

TABLE I. SUMMARY OF ACOUSTIC PARAMETERS IN FIGURES 1-9

Fig. #	Environments	P- (MPa)	Pulse Duration	PRF
1-2	Tissue-water	15.5	4-μs (3-cycle)	100 Hz
3-4	Inside Gel	> 21[a]	14-μs (10-cycle)	10 Hz
5-6	Tissue-water	> 21[a]	14-μs (10-cycle)	Single
7-8	Inside Gel	> 21[a]	14-μs (10-cycle)	Single
9	Gel & Gel-water	> 21[a]	14-μs (10-cycle)	10 Hz

a. The actual P- (peak negative pressure) at the focus could not be measured due to instantaneous onset of cavitation. P- at a lower power was measured to be 21 MPa.

B. Sample Preparation

Bubble clouds were generated at a tissue-water interface and inside an optically transparent gelatin phantom. The tissue sample was porcine atrial wall obtained fresh from a local abattoir (Northwest Meat Market, Jackson, MI USA) and used within 24h of harvesting. Gelatin phantoms (Type-A, Sigma-Aldrich, St. Louis, MO USA) with a concentration of 7% were used as a model for bulk tissue. Gel phantoms were stored at 4ºC overnight and warmed to room temperature before experiment the next day.

C. High Speed Imaging

The bubble cloud was imaged onto an ultrafast gated, intensified CCD (ICCD) camera (Picostar HR, La Vision, Goettingen, Germany). The intensifier uses a voltage gated microchannel plate (MCP) controlled via a high frame-rate imager (HRI). The output of the intensifier is coupled to a 640 x 480 pixel, 12-bit, 11 fps CCD camera storing up to 200 images at one time. To capture a snapshot of the bubble cloud

at a fixed delay after the arrival of the ultrasound pulse, the HRI was triggered by array driving software and an image was taken with a shutter speed of 100 – 200 ns.

Two types of bubble images were obtained. The whole bubble cloud was imaged with forward lighting and a field-of-view (FOV) of 3.6 x 2.7 cm. Shadowgraphs of individual bubbles were taken backlit with a compact long distance microscope (QM 100, Questar Corp., New Hope PA USA) over a 157 x 209 μm FOV. Ultrasound propagated from left to right in all the images.

The ICCD camera captures images by detecting and recording a count proportional to the photon number at each pixel. Pixels with bubbles have higher photon count (bright spots) in forward lighting image, and lower photon count (dark spots) in shadowgraphs. Therefore, we determine the first appearance of bubble cloud when the photon count exceeds a certain threshold for forward lighting imaging, and when the photon count falls below a certain threshold for shadowgraphs. Bubble cloud disappearance was determined by the opposite criteria. The threshold for bubble appearance is the mean + 3 SD values of noise for forward lighting imaging, and the mean – 3 SD for shadowgraph. The mean and standard deviation (SD) of photon count of the noise were computed using the images with no bubbles. These thresholds were applied to the total photon count to determine bubble cloud appearance, and to individual pixels to find pixels containing bubbles.

D. Acoustic Backscatter

Acoustic backscatter of therapy pulses from the focal zone was used to monitor the cavitation activity. To receive the acoustic backscatter, we mounted a 5-MHz, single element focused transducer (Valpey Fisher Corporation, Hopkinton, MA USA) confocally with the therapy array inside its inner hole. The 5-MHz transducer has a 25-mm diameter and a 100-mm focal length. Range-gated acoustic backscatter signals were collected by a digital oscilloscope (Model 9384L, LeCroy, Chestnut Ridge, NY USA) and processed by the Matlab program (Mathworks, Natick, MA USA).

Backscatter power and moving standard deviation (SD) were used to characterize the amplitude and variability of backscatter, respectively [4] (Fig. 1 e and f). The initiation and extinction of the temporally variable acoustic backscatter were detected based on the significantly increased and decreased temporal variability when initiation and extinction occur, respectively, as detailed in our previous paper [4].

III. RESULTS

A. Correlation between Acoustic Backscatter and Bubble Images

1) Tissue-water Interface: The appearance of the bubble cloud generated by ultrasound pulses correspond well to the initiation of the temporally changing acoustic backscatter, respectively (Fig. 1-2). The bubbles were not generated immediately at the arrival of the ultrasound pulses. It took 980 pulses until bubbles appeared. When no bubbles were seen in the shadowgraph, the backscatter was of lower amplitude and constant. When bubbles appeared, identified as significantly decreased photon count in the shadowgraph (Fig. 1b), the backscatter became high amplitude and temporally changing, determined by significantly increased backscatter power and SD (Fig. 1e-f). This provides support to our hypothesis that the backscatter is the sound reflection of the therapy pulses from a bubble cloud.

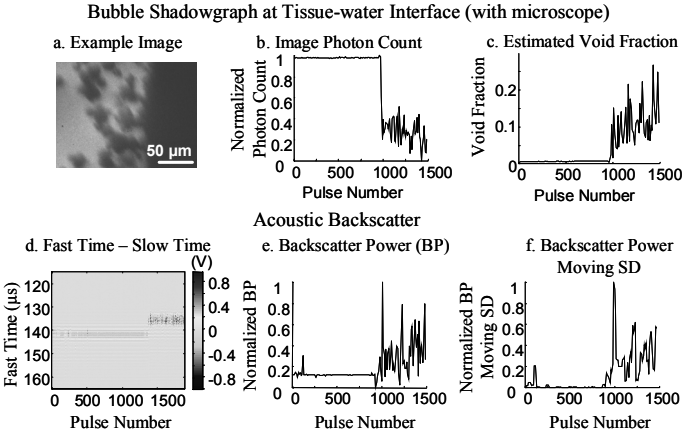

Figure 1. The first row shows an example of the bubble shadowgraph at a tissue-water interface, normalized total photon count and estimated void fraction vs. pulse number calculated based on the shadowgraph. The second row shows the simultaneously recorded acoustic backscatter in fast-time, slow-time display, backscatter power and SD vs. pulse number. The initiation of the acoustic backscatter matches the appearance of the bubble cloud. Ultrasound propagates from left to right in all the images.

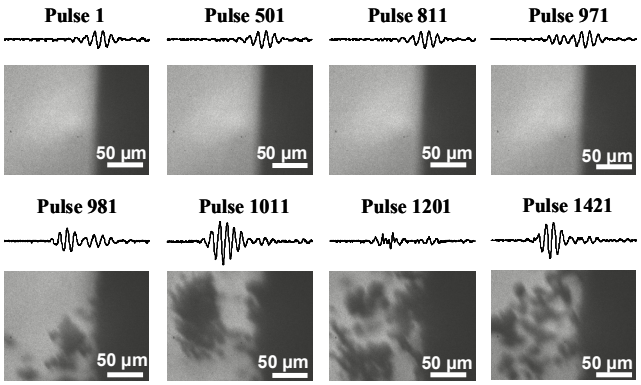

Figure 2. Actual waveforms of acoustic backscatter signal (top) and the corresponding bubble shadowgraph (bottom) at a tissue-water interface as in Fig. 1. The backscatter axes are the same as Fig. 1d. The tissue is the dark rectangular on the right and the bubble the dark spots against light background on the left. The acoustic backscatter was constant without bubbles (1st row), and temporally changing when bubbles were formed (2nd row).

2) Inside Gel: The disappearance of the bubble cloud generated by ultrasound pulses corresponds to extinction of the variable acoustic backscatter (Fig. 3-4). The gel is used as a model for bulk tissue. A bubble cloud was generated inside gel at the arrival of the ultrasound pulse. When the bubble cloud was seen, identified as a high total photon count in forward imaging, the acoustic backscatter power and SD were high (Fig. 3). After the 88th pulse, the ultrasound pulses could not generate new bubble clouds (Fig. 4), probably due to the depletion of cavitation nuclei inside the gel. Correspondingly, the acoustic backscatter became low amplitude and constant.

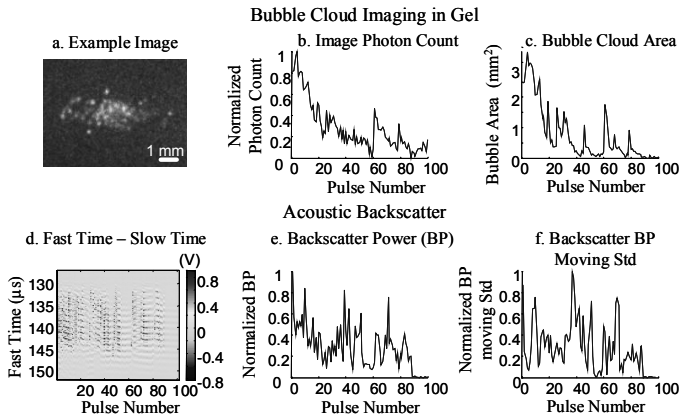

Figure 3. The first row shows a example of a bubble cloud image inside a gel, normalized total photon count and bubble cloud area vs. pulse number based on the imaging. The second row shows the simultanenously recorded acoustic backscatter in fast-time, slow-time display, backscatter power and SD vs. pulse number. The extinction of the acoustic backscatter matches the disappearance of the bubble cloud.

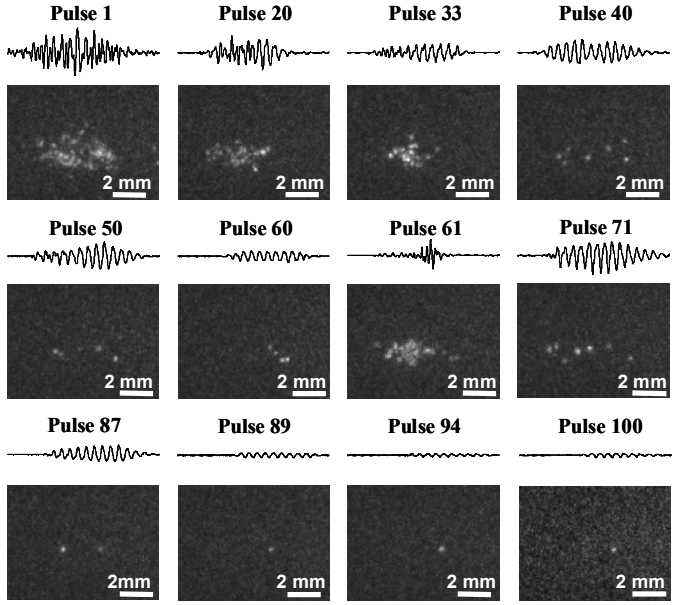

Figure 4. Actual waveforms acoustic backscatter signal (top) and the corresponding bubble image (bottom) produced inside a gel as in Fig. 3. The acoustic backscatter was high amplitude and changing when a bubble cloud was seen. After the 87th pulse, no bubble clouds were generated with only a residual bubble in the gel. Correspondingly, the acoustic backscatter is low amplitude and constant.

B. Temporal Change of Bubble Clouds

1) Tissue-water Interface: Images were taken at different times after the arrival of ultrasound pulse at a tissue-water interface (Fig. 5-6). A bubble cloud began to form at the arrival of the ultrasound pulse. It grew larger and denser with time during the pulse, and continued to grow long after the 14-μs pulse, up to at least 100μs. After that, the bubble cloud started to decay and lasted until about 300 μs. At 1 ms, no bubbles were recognized in forward lighting imaging or shadowgraphs. Small residual bubbles may still exist but were not imaged due to limited camera spatial resolution.

The bubble cloud appeared to be cone-shaped growing outward from the tissue surface. The cloud was ~5 mm long and ~4 mm wide at the base of the cone at its recorded peak size (100-μs). The bubble cloud was divided into sections about 1mm thick axially. Each section is seperated half of the wavelength at 750kHz, which suggests section formation is caused by a standing wave at the tissue boundary.

Individual bubbles 5-20 μm in diameter were observed in the bubble shadowgraph taken 1-μs after the arrival of the ultrasound pulse (Fig. 6). After that, bubble clouds grew denser with bubbles clustered and overlapped, making it hard to recognize individual bubble structure. At 100-μs, the bubble cloud became so dense that it often blocked all the light causing the shadowgraph to be completely dark (Fig. 6).

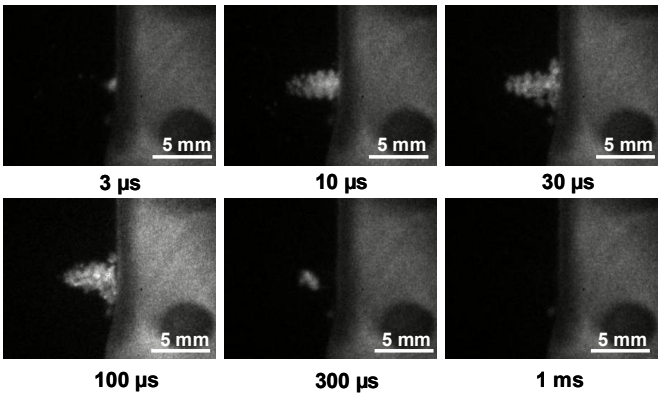

Figure 5. The bubble cloud images at a tissue-water interface with a fixed delay time after the arrival of the ultrasound pulse.

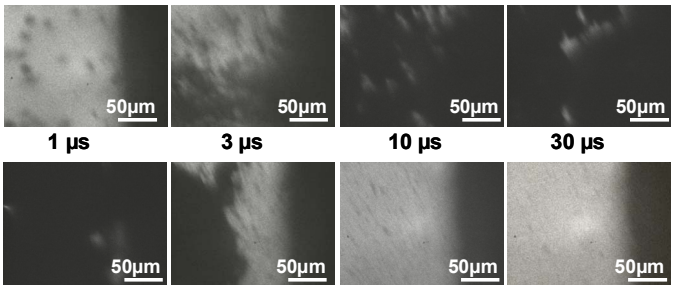

Figure 6. The bubble shadow at a tissue-water interface with a fixed delay time after the arrival of the ultrasound pulse. The shadowgraph at 100-μs is all dark because the bubble cloud is too dense bloking all the light.

2) Inside Gel: A bubble cloud started to form inside a gel at the arrival of the ultrasound pulse (Fig. 7-8). It grew larger and denser up to between 10 and 30-μs. The bubble cloud lasted until at least 100 μs, long after the 14-μs pulse ended. At 30-μs, the whole cloud was ~6 mm in length and ~2 mm in width, although the cloud seemed to separate into two portions in this example (Fig. 7).

The individual bubble growth can be seen clearly in the bubble shadowgraph in gel (Fig. 8). The diameter ranges of recognizable individual bubble structures were 6-10 μm at 1-μs, 12-27 μm at 3-μs, 18-45 μm at 30-μs, and 25-120 μm at 100-μs. At 10-μs, the bubble cloud is dense with bubbles clustered and overlapped, making it difficult to identify

individual bubbles. At 300-µs, no bubbles were recognized in forward lighting imaging or shadowgraphs.

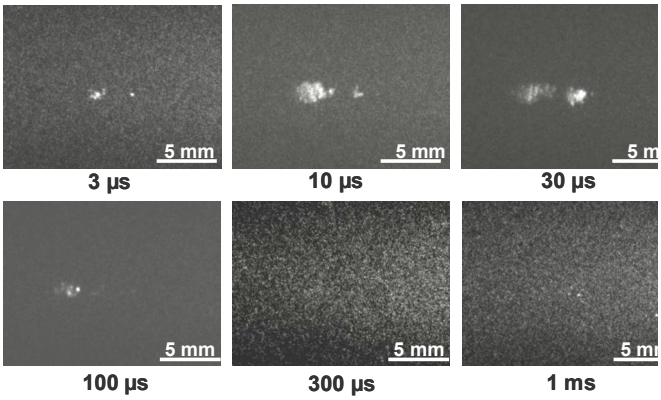

Figure 7. The bubble cloud images inside a gel with a fixed delay time after the arrival of the ultrasound pulse.

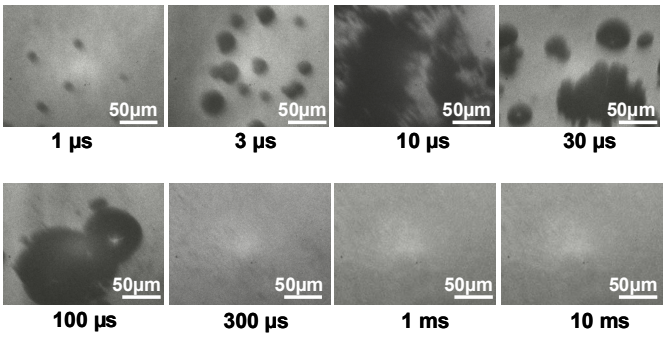

Figure 8. The bubble shwdowgraph inside a gel with a fixed delay after the arrival of the ultrasound pulse.

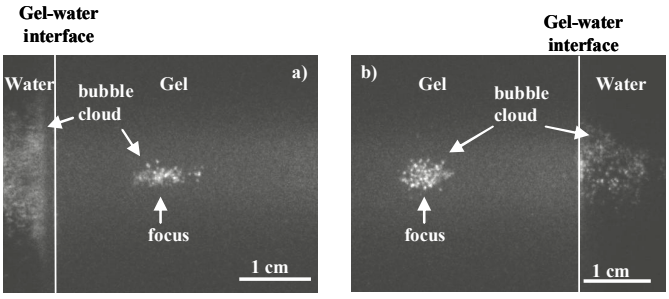

Figure 9. Images showing two bubble cloud were generated at the transducer focus inside the gel and at the gel-water interface ~1 cm pre-focus (left) and post-focus (right). However, no bubbles were generated between the focus and the gel-water interface, where the intensity is higher than that at age-water interface.

C. *Intensity Threshold*

The intensity threshold to generate a bubble cloud is higher inside the gel than at a gel-water interface. When focusing to generate a bubble cloud inside a gel, another bubble cloud was generated at the gel-water interface ~1 cm away from the focus, while no bubbles were created in between where the intensity was higher as it was closer to the focus (Fig. 9). This observation suggests a higher cavitation threshold in a bulk tissue than at a tissue-fluid interface. In addition, the bubble cloud generated at the gel-water interface was larger (Fig. 9) than that at the focus in the gel, even though the intensity was lower at the gel-water interface.

IV. Disscussion and Conclusions

Using high speed imaging, we observed that bubble clouds are generated by the short, high intensity ultrasound pulses at a tissue-water interface and inside a gel used to mimic bulk tissue. The appearance of this bubble cloud corresponds to the occurrence of a temporally changing acoustic backscatter of the therapy pulses, indicating that this backscatter is probably the sound reflection from this bubble cloud. As our previous studies have demonstrated that without the initiation of this backscatter pattern, tissue erosion and tissue liquefaction are never created [4, 5]. This result provides evidence that the cavitating bubble cloud plays a primary role in histotripsy.

Imaging shows that a bubble cloud generated by an ultrasound pulse of several µsec in duration grows larger and denser during and after the pulse, and can last for several hundreds of µsec. Individual bubbles start close to the resonant size (8-µm) corresponding to the transducer frequency (750-kHz), and grow larger over time even long after the pulse. Our previous optical monitoring results indicated that residual bubbles could remain for tens of msec [7], although the residual bubbles may be too small to be imaged due to our limited spatial resolution.

One interesting observation suggests a higher intensity threshold to initiate a bubble cloud in a bulk tissue than at a tissue-fluid interface, probably due to less cavitaton nuclei in tissue than fluid. This observation may explain the sharp boundary (several cell widths) observed in histotripsy generated tissue lesions [2, 3], in comparison to a few mm boundary of thermal lesions. The sharp boundary is most likely the result of a very large spatial threshold gradient.

Acknowledgment

The authors thank Dhruv Sud for his help with the imaging setup and Wei-Zung Chang for his input on data analysis. This research is funded by NIH grant R01 HL077629-01A1.

References

[1]. Z. Xu et al., "Controlled ultrasound tissue erosion," *IEEE Trans. Ultrason, Ferro. Freq. Control*, vol. 51, pp. 726-736, 2004.

[2]. W. W. Roberts et al., "Pulsed cavitational ultrasound: a noninvasive technology for controlled tissue ablation (histotripsy) in the rabbit kidney," *J. Urology*, vol. 175, pp. 734-8, 2006.

[3]. J. E. Parsons, C. A. Cain, G. D. Abrams, and J. B. Fowlkes, "Pulsed cavitational ultrasound therapy for controlled tissue homogenization," *Ultrasound Med. Biol.*, vol. 32, pp. 115-129, 2006.

[4]. Z. Xu, J. B. Fowlkes, E. D. Rothman, A. M. Levin, and C. A. Cain, "Controlled ultrasound tissue erosion: the role of dynamic interaction between insonation and microbubble activity," *J. Acoust. Soc. Am.*, vol. 117, pp. 424-435, 2005.

[5]. J. E. Parsons, J. B. Fowlkes, and C. A. Cain, "Acoustic backscatter features associated with production of tissue homogenate using pulsed cavitational ultrasound therapy," *Int. Symp. Therapeutic ultrasound*, pp. 323-327, 2005.

[6]. J. E. Parsons, C. A. Cain, and J. B. Fowlkes, "Cost-effective assembly of a basic fiber-optic hydrophone for measurement of high-amplitude therapeutic ultrasound fields," *J. Acoust. Soc. Am.*, vol. 119, pp. 1432-40, 2006.

[7]. Z. Xu, J. B. Fowlkes, and C. A. Cain, "Optical and acoustic monitoring of bubble dynamics at a tissue-fluid interface in ultrasound tissue erosion," *Int. Symp. Therapeutic ultrasound*, pp. 343-347, 2005.